ASSEMBLY INDUCED DELAMINATIONS IN COMPOSITE STRUCTURES[1]

J. Goering, R. Bohlmann, and Dr. S. Wanthal
McDonnell Aircraft Company
McDonnell Douglas Corporation, St. Louis, MO

E. Kautz
Naval Air Development Center, Warminster, PA

L. Neri
FAA Technical Center, Atlantic City, NJ

SUMMARY

Experimental and analytical studies of the development of delaminations around fastener holes in composite structures are presented. This type of delamination is known to occur in composite skins that are mechanically fastened to poorly mating substructure. Results of an experimental study to determine the resistance of laminates to the initiation of assembly induced delaminations and the residual strength of assembly damaged coupons are presented for AS4/3501-6, IM7/8551-7A, and AS4/PEEK material systems.

A survey of existing analytical models for predicting the residual strength and stability of delaminations is presented, and the development of a new model for predicting the initiation of delaminations around a fastener hole is outlined. The fastener hole damage initiation model utilizes a finite element based Fourier series solution, and is validated through comparisons of analytical and experimental results.

INTRODUCTION AND BACKGROUND

Two types of delaminations generally occur during the manufacture and assembly of composite aircraft structures; single level and multilevel delaminations. Single level delaminations are typically due to sources such as foreign objects between plies, disbonds during unbagging, thermal stresses during the cure cycle, or trapped voids. Multilevel delaminations are usually caused by an interlaminar failure at a fastener during assembly and will be addressed in this paper.

Assembly induced delaminations have been found on the AV-8B and F/A-18 aircraft. In both cases, the delaminations have occurred primarily at fasteners where gaps exist between surface skin and substructure. When the fastener is torqued up, the transverse load closes the unshimmed gap

---

[1] The analytical work described in this paper is being performed for the Naval Air Development Center and the Federal Aviation Administration under contract N62269-90-C-0281, 'Delamination Methodology for Composite Structure.'

and, if the gap is too large, creates a delamination in either the skin, the substructure, or both depending on the relative stiffnesses and strengths of the elements.

Delaminations of this type were first found on the AV-8B in the upper compression skin of the wing near the inboard pylon, Figure 1. The delaminations were caused by gaps between the skin and substructure that were not shimmed. The maximum gap condition occurred at the inboard pylon location where a composite sinewave spar intersects a composite rib with aluminum fittings (Figure 2). As shown in Figure 3, a close up view of a straight edge laid across a spar reveals a significant gap. When large gaps are not properly shimmed and fasteners are installed, delaminations will result as shown by the ultrasonic inspection of the skin at the inboard pylon (Figure 4). The delamination encompasses several fastener holes. The gap condition at this location was significantly improved by modifying the manufacturing process for the wing assembly. This included changing the procedure for using liquid shim, as well as changes in tooling and detail geometry changes in the metal and composite parts. Other issues besides unshimmed gaps at fastener holes can cause delaminations during assembly (Figure 5), but these causes were not found to be as significant as unshimmed gaps.

A methodology, which includes analysis methods to predict the post-delamination response of damaged laminates, is needed to establish criteria for acceptance, rejection, or repair of delaminated structures. McDonnell Aircraft Company (MCAIR) is currently conducting a research and development program for the Naval Air Development Center and the Federal Aviation Administration to develop such a methodology. The approach being pursued in this program is to: 1 - rely on MCAIR's existing test database to help characterize and idealize the details of typical damage; 2 - use existing analytical models for predicting local stability, strength failures, and crack growth in laminates containing idealized damage whenever possible; and 3 - develop new special purpose analyses when there are deficiencies in the existing models.

The relationship of the analysis model to the damage detected is the key to successfully predicting the response of the structure with the defect in place. An A-Scan of the delaminated area around a fastener hole in a fastener torque-up specimen is illustrated in Figure 6, and shows the damage is actually a series of elliptical delaminations stacked through the thickness of the laminate. The complex nature of fastener induced delamination is further demonstrated by the photomicrograph shown in Figure 7. Several delaminations are clearly visible and there is considerable transverse matrix cracking. Transverse matrix cracks can grow through plies until they reach an interface and then grow as a delamination, which may not extend to free surfaces.

EXPERIMENTAL STUDY

A test program was initiated at MCAIR to evaluate the delamination resistance and damage tolerance of several thermoset and thermoplastic material systems which show potential for use in advanced aircraft

structure. The goal was to understand the initiation of assembly induced delaminations and to identify delamination mechanisms in tough composite materials. The material systems chosen for this study were: the baseline epoxy system used on the AV-8B and F/A-18 (AS4/3501-6), a toughened epoxy (IM7/8551-7A), and a thermoplastic (AS4/PEEK). The general test plan for the AS4/PEEK and AS4/8551-7A specimen is summarized in Figure 8.

Each material system was used to manufacture test panels of equal thickness (.224 in.) and identical stacking sequence using combinations of 0, ±22.5, ±45, ±67.5, and 90 degree plies. After fabrication, the panels were machined into rectangular compression test specimens (Figure 9a) and fasteners were installed to simulate the spar/rib intersections where assembly induced delaminations frequently occur. Cross section specimens were also fabricated (Figure 9b)to evaluate the microstructure at a delamination by obtaining photomicrographs of the edge of the delamination. The delaminations were viewed at 0, 45, and 90 degree cuts through the delamination.

The test setup used to produce the delaminations is shown in Figure 10. The fastener is tightened by a torque wrench from the countersunk side of the fastener, similar to the production situation. The specimen is supported by ~3 in. diameter pipe. A load cell and a deflectometer were included in the setup so that specimen load deflection plots were obtained for each material system, as shown in Figure 11. The toughened thermoset IM7/8551-7A specimens delaminated at 32% higher load than the baseline AS4/3501-6 material, and the AS4/PEEK thermoplastic specimens delaminated at a load 67% higher than the baseline. The deflection of the thermoplastic specimens were nearly double the baseline panel when delamination occurred. This indicates that the thermoplastic material is more damage resistant and could withstand twice the unshimmed gap prior to delamination occurring.

Static strength and fatigue tests were planned on baseline (no delamination) and delaminated panels. The post delamination static compression strength of all three materials is compared to their baseline undelaminated strengths in Figure 12. The delamination size for the AS4/PEEK was larger (~2 in. dia.) than the IM7/8551-7A (~1.5 in. dia.) but the percentage reduction in compression strength from the undelaminated cases are equivalent. Compression fatigue testing with and without assembly induced delaminations is currently in progress.

ANALYTICAL MODELS

A thorough analytical investigation of assembly induced delaminations must address three problems; 1 - defining the conditions under which a delamination will be initiated, and the size of the initial delamination, 2 - determining the residual strength of a laminate which includes a delamination, and 3 - determining if an existing delamination will grow when the laminate is loaded. Most of the analytical work performed to date has concentrated on the second and third problems, and has considered damage due to low velocity impact events rather than assembly induced damage. In many cases, however, the models intended for low

velocity impact damage can be used to study assembly induced damage with little or no modification.

Review of Existing Delamination Models

In general, existing delamination analyses study one or more of three basic failure modes; 1 - static failure in or near the delaminated region, 2 - buckling of one or more of the sublaminates created by the delamination, and/or 3 - delamination growth caused by static or buckling-induced loads. These three modes can work in conjunction to cause a catastrophic failure.

Most of the previous works have considered very specialized cases, assuming such things as orthotropic materials, pure compression loads, etc. In addition, much of this work considers only single level delaminations, even though impact and assembly induced damage is typically characterized by multiple level delaminations. Only a few researchers have provided fairly comprehensive discussions of more generalized analysis methods [1,2].

A large percentage of the single level delamination work involves the use of 2-D and 3-D finite element analysis to predict the onset and growth of delaminations [3-14]. These predictions are generally made through strain energy release rate calculations. The finite element analyses generally show good agreement with test data, but are relatively time-consuming to perform.

Several simplified solutions for flat laminates containing single level delaminations also exist. These analyses fall into one of three general groups; 1 - edge delamination analyses [11,15-17], 2 - through-width delamination analyses [2,18-23], and 3 - embedded delamination analyses [1,2,7,11,24-28].

Edge delaminations are generally caused by tensile loading. Since free edges of a laminate under tensile loading must be stress-free, out of plane stress concentrations develop near the edges, which can cause the plies to delaminate. Pipes and Pagano [15] presented a well known solution for these interlaminar stresses near a free edge in cross plied laminates which was later extended to more general laminates [16]. Damage growth predictions for edge delaminations have been made by Wilt, et al [11] using the finite element method; and Armanios, et al [17] developed a shear deformable plate model to predict stresses near the edge delamination tip.

Many researchers have investigated analytical models of through-width delaminations, which are used to predict sublaminate buckling and/or growth of the delamination. These models present less formidable analytical challenges since they represent what are essentially two dimensional problems, but are less representative of actual aircraft damage scenarios than edge and embedded delamination models. Whitcomb [5] used finite elements to perform parametric studies on the growth of through-width delaminations loaded into a postbuckled state and, in another paper [18], used a simplified Rayleigh-Ritz model to perform a parametric study of the stability of sublaminates which included thermal

effects. Vizzini and Lagace [19] developed a sublaminate buckling model which included the effects of an elastic foundation on the response.

Yin [20] presented a closed form solution for buckling of through-width delaminations under combined in-plane loading. Yin also presents an expression for strain energy release rate for the combined load case. Kardomateas [21] also presented a closed form solution for local and global buckling of through-width delamination under axial compression only. Martin [22] used a combination of curved beam elasticity solutions and finite element models to predict the onset and growth of delamination in unidirectional curved laminates. Sankar [23] presented a specialized beam finite element which was used to calculate strain energy release rates.

The third and most common type of delamination is an embedded delamination. Residual strength models have typically modeled embedded delaminations as elliptic inclusions in a parent (undamaged) laminate. Lekhnitskii [24] solved this problem for the stresses in and around the inclusion, and his solution has served as the basis for many subsequent models. Cairns [1,25] used Lekhnitskii's solution as part of a larger effort to predict the damage resistance and damage tolerance of laminates subject to low velocity impact. Cairns also presented an assumed-modes Rayleigh-Ritz method for predicting sublaminate buckling. Several other authors [2,7,24-28] have developed models for predicting buckling loads of elliptical delaminations making use of varying assumptions about loading, geometry, and material symmetry.

In general the delaminated sublaminates will not be symmetric or balanced and the associated coupling effects should be included in the buckling load calculations. A simple way of estimating these coupling effects is to modify the bending terms using a reduced bending stiffness (RBS) approach [29-31]. This method involves inverting the full 6 x 6 matrix formed by the A, B and D matrices from laminated plate theory, to include effects of the A and B matrices in the D matrix coefficients.

When a sublaminate buckles it experiences an out-of-plane displacement which in turn induces out-of-plane loads at the perimeter of the delamination. If these loads are large enough, the delamination will grow. Various methods have been studied to predict this delamination growth. The most common of these is to calculate the strain energy release rates for an assumed delamination growth [2,5,13,14,21,32-34]. This rate is then compared with material property data to determine the load at which growth will occur. Cairns [25] suggests the use of Marguerre initial imperfection theory to calculate stresses at the boundary of the sublaminate. A strength of materials approach is then used to predict delamination growth.

Although these embedded delamination models were originally formulated for single level delaminations, they can be extended to analyze the multiple level delamination case. This is typically done by combining one of the Rayleigh-Ritz buckling analyses with Lekhnitskii's elliptical inclusion model. The delaminations are assumed to divide the laminate into several elliptical sublaminates. The strength of the delaminated region is then found by analyzing the response of each individual

sublaminate. When an instability failure (sublaminate buckling) is predicted in a sublaminate, it can carry no additional load and in effect becomes a reduced stiffness inclusion. Any additional load must be sheared around the inclusion or redistributed to other sublaminates. If a strength failure is predicted the sublaminate can carry no load, and the existing load must be redistributed to other sublaminates. Using this approach, the load is applied incrementally, and the progression of sublaminate failures are tracked until all sublaminates have experienced strength failures.

Fastener Hole Damage Initiation Model

The existing analytical models are useful for predicting the effects of delaminations on the response of uniform continuous laminates. In the case of assembly induced damage, however, delaminations typically occur around structural details such as fastener holes. Models which predict the initiation of delaminations around fastener holes have been developed [35,36], but they only consider in plane tensile loads and do not account for out of plane loads due to the fastener.

As a first step toward developing a comprehensive model for analyzing the effect of delaminations around fastener holes, MCAIR has developed a damage initiation model that considers out-of-plane loads. This model represents an annulus of orthotropic material around a countersunk fastener hole, as shown in Figure 13. The annulus is modeled in two dimensions using a special purpose anisotropic harmonic axisymmetric finite element that was developed specifically for this analysis.

The anisotropic harmonic axisymmetric element assumes that the geometry of the element is truly axisymmetric, but allows the material properties and strain fields to vary in the circumferential direction. Degrees of freedom associated with the element are translations in the radial, circumferential, and axial directions at each node (**u**, **v**, and **w**, respectively). To retain generality in the circumferential variations of the displacements, they are expressed as Fourier series in θ. The three dimensional displacement fields for the element are then given by:

$$u = u_o + \sum_{i=1}^{\infty}(u'_i \cdot \cos(i\theta) + u''_i \cdot \sin(i\theta)) \quad (1)$$

$$v = v_o + \sum_{i=1}^{\infty}(v'_i \cdot \sin(i\theta) - v''_i \cdot \cos(i\theta)) \quad (2)$$

$$w = w_o + \sum_{i=1}^{\infty}(w'_i \cdot \cos(i\theta) + w''_i \cdot \sin(i\theta)) \quad (3)$$

Where u_o, v_o, w_o, u'_i, v'_i, w'_i, u''_i, v''_i, and w''_i are functions of R and Z only. The primed displacement components correspond to modes that are symmetric with respect to the $\theta = 0$ plane, and the double primed components correspond to asymmetric modes.

Since three dimensional displacement fields are assumed, all six strain components may develop. In cylindrical coordinates, these strain components are defined as:

$$\varepsilon = \begin{Bmatrix} \varepsilon_{rr} \\ \varepsilon_{\theta\theta} \\ \varepsilon_{zz} \\ \gamma_{r\theta} \\ \gamma_{\theta z} \\ \gamma_{zr} \end{Bmatrix} = \begin{Bmatrix} \dfrac{\partial u}{\partial r} \\ \dfrac{u}{r} + \dfrac{1}{r}\dfrac{\partial v}{\partial \theta} \\ \dfrac{\partial w}{\partial z} \\ \dfrac{\partial v}{\partial r} - \dfrac{v}{r} + \dfrac{1}{r}\dfrac{\partial u}{\partial \theta} \\ \dfrac{1}{r}\dfrac{\partial w}{\partial \theta} + \dfrac{\partial v}{\partial z} \\ \dfrac{\partial u}{\partial z} + \dfrac{\partial w}{\partial r} \end{Bmatrix} \tag{4}$$

Substituting (1), (2), and (3) into (4) yields a general expression for the three dimensional strain field

$$\varepsilon = \varepsilon_o + \sum_{i=1}^{\infty} (\varepsilon'_i + \varepsilon''_i) \tag{5}$$

Where

$$\varepsilon_o = \begin{bmatrix} \dfrac{\partial}{\partial r} & 0 & 0 \\ \dfrac{1}{r} & 0 & 0 \\ 0 & 0 & \dfrac{\partial}{\partial z} \\ 0 & \dfrac{1}{r} - \dfrac{\partial}{\partial r} & 0 \\ 0 & -\dfrac{\partial}{\partial z} & 0 \\ \dfrac{\partial}{\partial z} & o & \dfrac{\partial}{\partial r} \end{bmatrix} \begin{Bmatrix} u_o \\ v_o \\ w_o \end{Bmatrix} \tag{6}$$

$$\varepsilon'_i = \begin{bmatrix} \cos(i\theta)\dfrac{\partial}{\partial r} & 0 & 0 \\ \cos(i\theta)\cdot\dfrac{1}{r} & \cos(i\theta)\cdot\dfrac{i}{r} & 0 \\ 0 & 0 & \cos(i\theta)\dfrac{\partial}{\partial z} \\ -\sin(i\theta)\cdot\dfrac{i}{r} & -\sin(i\theta)\cdot\left(\dfrac{1}{r} - \dfrac{\partial}{\partial r}\right) & 0 \\ 0 & \sin(i\theta)\dfrac{\partial}{\partial z} & -\sin(i\theta)\cdot\dfrac{i}{r} \\ \cos(i\theta)\dfrac{\partial}{\partial z} & 0 & \cos(i\theta)\dfrac{\partial}{\partial r} \end{bmatrix} \begin{Bmatrix} u'_i \\ v'_i \\ w'_i \end{Bmatrix} \tag{7}$$

and

$$\varepsilon''_i = \begin{bmatrix} \sin(i\theta)\cdot\frac{\partial}{\partial r} & 0 & 0 \\ \sin(i\theta)\cdot\frac{1}{r} & \sin(i\theta)\cdot\frac{i}{r} & 0 \\ 0 & 0 & \sin(i\theta)\cdot\frac{\partial}{\partial z} \\ \cos(i\theta)\cdot\frac{i}{r} & \cos(i\theta)\cdot\left(\frac{1}{r} - \frac{\partial}{\partial r}\right) & 0 \\ 0 & -\cos(i\theta)\cdot\frac{\partial}{\partial z} & \cos(i\theta)\cdot\frac{i}{r} \\ \sin(i\theta)\cdot\frac{\partial}{\partial z} & 0 & \sin(i\theta)\cdot\frac{\partial}{\partial r} \end{bmatrix} \begin{Bmatrix} u''_i \\ v''_i \\ w''_i \end{Bmatrix} \qquad (8)$$

The geometry of the element is defined by twelve nodes in the R-Z plane, which represent an annulus of material, as shown in Figure 14. Displacements throughout the domain of the element are approximated using interpolation functions of the form

$$f(r,z) = \sum_{n=1}^{12} h_n(r,z) \cdot f_n \qquad (9)$$

Where the h_n are coefficients in the cubic interpolation function for an ordinary two dimensional 'serendipity' type element, and f_n is the displacement at node n.

Approximating u_o, v_o, w_o, u'_i, v'_i, w'_i, u''_i, v''_i, and w''_i using (9), and substituting into (6), (7), and (8) provides an expression for the strain throughout the element in terms of the nodal displacements.

$$\varepsilon = \mathbf{B}_o \begin{Bmatrix} u_{o_1} \\ v_{o_1} \\ w_{o_1} \\ \cdot \\ \cdot \\ \cdot \\ u_{o_{12}} \\ v_{o_{12}} \\ w_{o_{12}} \end{Bmatrix} + \sum_{i=1}^{\infty} \mathbf{B}'_i \begin{Bmatrix} u'_{i_1} \\ v'_{i_1} \\ w'_{i_1} \\ \cdot \\ \cdot \\ \cdot \\ u'_{i_{12}} \\ v'_{i_{12}} \\ w'_{i_{12}} \end{Bmatrix} + \mathbf{B}''_i \begin{Bmatrix} u''_{i_1} \\ v''_{i_1} \\ w''_{i_1} \\ \cdot \\ \cdot \\ \cdot \\ u''_{i_{12}} \\ v''_{i_{12}} \\ w''_{i_{12}} \end{Bmatrix} = \mathbf{B} \cdot \mathbf{u} \qquad (10)$$

The constitutive law for the laminates considered in this program will be constant when expressed in rectangular coordinates, and is defined by

$$\sigma^* = \mathbf{D}^* \cdot \varepsilon^* \qquad (11)$$

where

$$\varepsilon^* = \begin{Bmatrix} \varepsilon_{xx} \\ \varepsilon_{yy} \\ \varepsilon_{zz} \\ \gamma_{xy} \\ \gamma_{yz} \\ \gamma_{zx} \end{Bmatrix} \quad , \quad \sigma^* = \begin{Bmatrix} \sigma_{xx} \\ \sigma_{yy} \\ \sigma_{zz} \\ \tau_{xy} \\ \tau_{yz} \\ \tau_{zx} \end{Bmatrix} \tag{12,13}$$

and $\mathbf{D}^*$ is a 6 X 6 matrix that can be, in general, fully populated. The constitutive law in cylindrical coordinates is calculated from (11), using the strain transformation defined by

$$\varepsilon = \mathbf{T} \cdot \varepsilon^* \tag{14}$$

where

$$\mathbf{T} = \begin{bmatrix} \cos^2\theta' & \sin^2\theta' & 0 & \sin\theta'\cdot\cos\theta' & 0 & 0 \\ \sin^2\theta' & \cos^2\theta' & 0 & -\sin\theta'\cdot\cos\theta' & 0 & 0 \\ 0 & 0 & 1 & 0 & 0 & 0 \\ -2\cdot\sin\theta'\cdot\cos\theta' & 2\cdot\sin\theta'\cdot\cos\theta' & 0 & \cos^2\theta'-\sin^2\theta' & 0 & 0 \\ 0 & 0 & 0 & 0 & \cos\theta' & -\sin\theta' \\ 0 & 0 & 0 & 0 & \sin\theta' & \cos\theta' \end{bmatrix} \tag{15}$$

and

$$\theta' = \theta - \beta \tag{16}$$

Substituting (14) and a similar transformation for stress into (11) yields

$$\sigma = \mathbf{D} \cdot \varepsilon \tag{17}$$

where

$$\sigma = \begin{Bmatrix} \sigma_{rr} \\ \sigma_{\theta\theta} \\ \sigma_{zz} \\ \tau_{r\theta} \\ \tau_{\theta z} \\ \tau_{zr} \end{Bmatrix} \tag{18}$$

and $\mathbf{D}$ is a θ dependent expression given by

$$\mathbf{D} = \mathbf{T}^T \cdot \mathbf{D}^* \cdot \mathbf{T} \tag{19}$$

Using standard finite element procedures [37], the effective stiffness of the element is calculated by minimizing the potential energy, which is defined in terms of the nodal unknowns using (10) and (17).

$$\mathbf{K} = \int_{vol} \mathbf{B}^T \cdot \mathbf{D} \cdot \mathbf{B} \, dv \tag{20}$$

Unlike conventional axisymmetric and isotropic or cylindrically orthotropic harmonic axisymmetric elements, integrating (20) in the circumferential direction is not trivial, and must be performed numerically. In addition, the anisotropic nature of $\mathbf{D}$ leads to coupling between the modes of the Fourier series that does not exist for isotropic or cylindrically orthotropic elements. Each element in a model that considers j modes will then have $(36 + 72 \cdot j)$ degrees of freedom, consisting of u_0, v_0, and w_0 at each node, and u'_j, v'_j, w'_j, u''_j, v''_j, and w''_j for each mode at each node.

Since the element uses cubic interpolation functions in the R-Z plane, the geometry shown in Figure 13 can be modeled with a relatively coarse mesh. The number of terms in the Fourier series required to characterize circumferential variations depends on the degree of anisotropy of $\mathbf{D}^*$ and on the applied load. Two different load cases can be considered, one represents a properly seated fastener and the other represents an improperly seated fastener (Figure 15). For the properly seated case the normal pressure on the countersink is assumed to be constant in θ, and for the improperly seated case it is defined by

$$P(\theta) = P \cdot (1 + \cos(\theta)) \tag{21}$$

The number of terms in the Fourier series for various material types and loads cases is listed in Table 1. In practice, the solution predicted by this model converges very rapidly, and only a few terms in the Fourier series are required. A convergence study was performed for a .1040 inch thick AS4/3501-6 laminate with a $[(\pm 67.5)2/90/45/(-45)2/(0)2]_S$ stacking sequence. This study showed that the displacement solution converged to within .001% using only three terms in the series.

Results predicted by the model have been compared to some of the experimental results described above. Comparisons of the analytically and experimentally determined effective stiffnesses for AS4/3501-6, IM7/8551-7A, and AS4/PEEK laminates are shown in Figure 16. The geometrical parameters and stacking sequence used for these analyses are listed in Table 2. For these comparisons, the effective stiffness of each laminate was taken as the axial load in the fastener divided by the maximum lateral deflection of the laminate. As shown in Figure 16, there is very good agreement between the experimental and analytical results.

The initiation of damage in the AS4/3501-6 laminate was also predicted analytically, based on the average stresses calculated over a characteristic length away from the fastener hole. For this analysis, it

was assumed that ply interfaces were isotropic matrix rich regions, and that a delamination would occur when the von Mises stress in an interface exceeded the shear strength of the matrix. Since the stress and strain fields are three dimensional, each interface was searched in the circumferential direction to identify the critical location for the initiation of damage, and the radial length of the element closest to the fastener hole was used as the characteristic length. The predicted damage initiation load as a function of the characteristic length is shown in Figure 17, along with experimental data for the same laminate. The properly and improperly seated cases bracket the experimental data very well, and the properly seated case is tending toward the experimental result as the characteristic length approaches zero. The failure predicted by the analysis was at a circumferential location approximateley 45° away from the 0° direction of the laminate and just below the bottom of the countersink, which corresponds well with the observed failure.

DISCUSSION AND CONCLUSIONS

The results of the experimental study indicate that it may be possible to improve the resistance of aircraft to assembly induced delaminations by using a tough epoxy or thermoplastic material system. The fastener loads required to cause delaminations in these systems were 32% and 67% higher than the initial delamination load for the conventional epoxy system. The fact that the toughened epoxy and thermoplastic specimens experienced larger lateral deflections before delaminating implies that structure fabricated from these materials can tolerate larger unshimmed gaps than similar structures fabricated from conventional epoxy. Strength reductions due to the presence of delaminations in the tougher systems were comparable to the reduction observed for conventional epoxy specimens, although the thermoplastic does start from a baseline strength that is below that for either thermoset system.

The survey of existing analytical methods shows that while a significant amount of research has been conducted to develop models for studying delaminations in general, very little work has been done on the specific problem of analyzing delaminations around fastener holes. The existing sublaminate buckling and elliptical inclusion models for analyzing the response of a laminate with an embedded delamination subject to in-plane loads may be used to study the effects of delaminations around fastener holes. However, they must be modified to account for the additional constraint the fastener places on the buckled mode shape, and for the stress concentration due to the fastener hole. The existing fracture mechanics approaches to predict the growth of these delaminations will require similar modifications.

Finite element based solutions appear to be the most appropriate methods for analyzing fastener induced delaminations subject to out-of-plane loads, such as those due to the fastener itself. The anisotropic harmonic axisymmetric element developed at MCAIR provides a means for efficiently modeling this problem. This approach has been demonstrated to accurately predict both the location and load required to produce the

initial delamination. This same model can be used to explicitly model delaminations by treating the elliptical delamination as an effective circular delamination. It may also be possible to use this model to numerically determine strain energy release rates as part of a methodology to predict the growth of an existing delamination.

REFERENCES

[1] Cairns, D. S., "Impact and Post-Impact Response of Graphite/Epoxy and Kevlar/Epoxy Structures," TELAC Report 87-15, Massachusetts Institute of Technology, August, 1987.

[2] Kan, H.P. and Graves, M.J., "Damage Tolerance of Composites - Volume III. Analysis, Methods, Development, and Test Verification," AFWAL-TR-87-3030, Vol. III, July, 1988.

[3] Wilkins, D.J., Eisenmann, J.R., Camin, R.A., Margolis, W.S., and Benson, R.A., "Characterizing Delamination Growth in Graphite-Epoxy," Damage in Composite Materials, ASTM STP 775, pp. 184-210, 1980.

[4] O'Brien, T.K., "Characterization of Delamination Onset and Growth in a Composite Laminate," Damage in Composite Materials, ASTM STP 775, pp. 184-210, 1980.

[5] Whitcomb, J.D., "Finite Element Analysis of Instability Related Delamination Growth," Journal of Composite Materials, Vol. 15, pp. 403-426, September, 1981.

[6] Ericson, K., Persson, M., Carlsson, L. and Gustavsson, A., "On the Prediction of the Initiation of Delamination in a [0/90]s Laminate with a Circular Hole," Journal of Composite Materials, Vol. 18, pp. 495-506, September, 1984.

[7] Shivakumar, K.N. and Whitcomb, J.D., "Buckling of a Sublaminate in a Quasi-Isotropic Composite Laminate," Journal of Composite Materials, Vol. 19, pp. 2-18, January, 1985.

[8] Donaldson, S.L., "The Effects of Interlaminar Fracture Properties on the Delamination Buckling of Composite Laminates," Composites Science and Technology, Vol. 28, pp. 33-44, 1987.

[9] Sun, C.T. and Kelly, S.R., "Failure in Composite Angle Structures Part I: Initial Failure," Journal of Reinforced Plastics and Composites, Vol. 7, pp. 220-232, May, 1988.

[10] Sun, C.T. and Kelly, S.R., "Failure in Composite Angle Structures Part II: Onset of Delamination," Journal of Reinforced Plastics and Composites, Vol. 7, pp. 233-244, May, 1988.

[11] Wilt, T.E., Murthy, P.L.N. and Chamis, C.C., "Fracture Toughness Computational Simulation of General Delaminations in Fiber Composites," Journal of Reinforced Plastics and Composites, Vol. 8, pp. 2-17, January, 1989.

[12] Shaw, D. and Tsai, M.Y., "Analysis of Delamination in Compressively Loaded Laminates," Composites Science and Technology, Vol. 34, pp. 1-17, 1989.

[13] Whitcomb, J.D. and Shivakumar, K.N., "Strain-Energy Release Rate Analysis of Plates with Postbuckled Delaminations," Journal of Composite Materials, Vol. 23, pp. 714-734, July, 1989.

[14] Whitcomb, J.D., "Three-Dimensional Analysis of a Postbuckled Embedded Delamination," Journal of Composite Materials, Vol. 23, pp. 862-889, September, 1989.

[15] Pipes, R.B. and Pagano, N.J., "Interlaminar Stresses in Composite Laminates Under Uniform Axial Extension," Journal of Composite Materials, Vol. 4, pp. 538-548, October 1970.

[16] Pagano, N.J. and Pipes, R.B., " The Influence of Stacking Sequence on Laminate Strength," Journal of Composite Materials, Vol. 5, pp. 50-57, January 1971.

[17] Armanios, E.A., Badir, A. and Sriram, P., "Sublaminate Analysis of Mode I Edge Delamination in Laminated Composites," AIAA, paper no. 89-1401-CP, 1989.

[18] Whitcomb, J.D., "Parametric Analytical Study of Instability-Related Delamination Growth," Composites Science and Technology, Vol. 25, pp. 19-48, 1986.

[19] Vizzini, A.J. and Lagace, P.A., "The Buckling of a Delaminated Sublaminate on an Elastic Foundation," Journal of Composite Materials, vol. 21, pp. 1106-1117, December, 1987.

[20] Yin, W.L., "The Effects of Laminated Structure on Delamination Buckling and Growth," Journal of Composite Materials, Vol. 22, pp. 502-517, June, 1988.

[21] Kardomateas, G.A., "End Fixity Effects on the Buckling and Post-Buckling of Delaminated Composites," Composites Science and Technology, Vol. 34, pp. 113-128, 1989.

[22] Martin, R. H., "Delamination Failure in a Unidirectional Curved Composite Laminate," 10th ASTM Symposium on Composite Materials: Testing and Design, April, 1990.

[23] Sankar, B.V., "A Finite Element for Modeling Delaminations in Composite Beams," Computers and Structures, Vol. 38, No. 2, pp 239-246, 1991.

[24] Lekhnitskii, S.G., Anisotropic Plates, Translated by S.W. Tsai and T. Cheron, Gordon and Breach Science Publishers, New York, 1968.

[25] Cairns, D. S., "Simple Criteria for Delamination Growth as a Result of Sublaminate Buckling - Theoretical Basis," TELAC Report 87-15, Massachusetts Institute of Technology, 1987.

[26] Horban, B. and Palazotto, A., "The Experimental Buckling of Cylindrical Composite Panels with Eccentrically Located Circular

Delaminations," Proceedings of the 27th. AIAA/ASME/ASCE/AHS Structures, Structural Dynamics, and Materials Conference, pp. 159-164, 1986.

[27] Kassapoglou, C., "Buckling, Post-Buckling and Failure of Elliptical Delaminations in Laminates under Compression," Composite Structures, Vol. 9, pp. 139-159, 1988.

[28] Chai, H. and Babcock, C. D., "Two-Dimensional Modelling of Compressive Failure in Delaminated Laminates," Journal of Composite Materials, Vol. 19, pp. 67-98, January, 1985.

[29] Chamis, C.C., "Buckling of Anisotropic Composite Plates," Journal of the Structural Division, Proceedings of the ASCE, Vol. 95, pp. 2119-2139, 1969.

[30] Jensen, D. W. and Lagace, P. A., "Influence of Mechanical Couplings on the Buckling and Postbuckling Behavior of Anisotropic Plates," AIAA Proceedings 86-0880, 1986.

[31] Ewing, M.S., Hinger, R.J., and Leissa, A.W., "On the Validity of the Reduced Bending Stiffness Method for Laminated Composite Plate Analysis," Composite Structures, Vol. 9, pp. 301-317, 1988.

[32] Sriram, P. and Armanios, E.A., "Fracture Analysis of Local Delaminations in Laminated Composites," AIAA paper no, 89-1400-CP, 1989.

[33] Chen, E.P. and Sih, G.C., "Interfacial Delamination of a Layered Composite Under Anti-Plane Strain," Journal of Composite Materials, Vol. 5, pp. 12-23, January, 1971.

[34] Chatterjee, S.N., Dick, W.A. and Pipes, R.B., "Mixed-Mode Delamination Fracture in Laminated Composites," Composites Science and Technology, Vol. 25, pp. 49-67, 1986.

[35] Ye, L. "Characteristics of Delamination Growth in a Notched Graphite/Epoxy Composite Laminate," Journal of Reinforced Plastics and Composites, Vol. 8, pp. 79-90, January, 1989.

[36] Shalev, D. and Reifsnider, K.L., "Study of the Onset of Delamination at Holes in Composite Laminates," Journal of Composite Materials, Vol. 24, pp. 42-71, January, 1990.

[37] Zienkiewicz, O.C., The Finite Element Method, McGraw-Hill Book Company (UK) Limited, London, 1977.

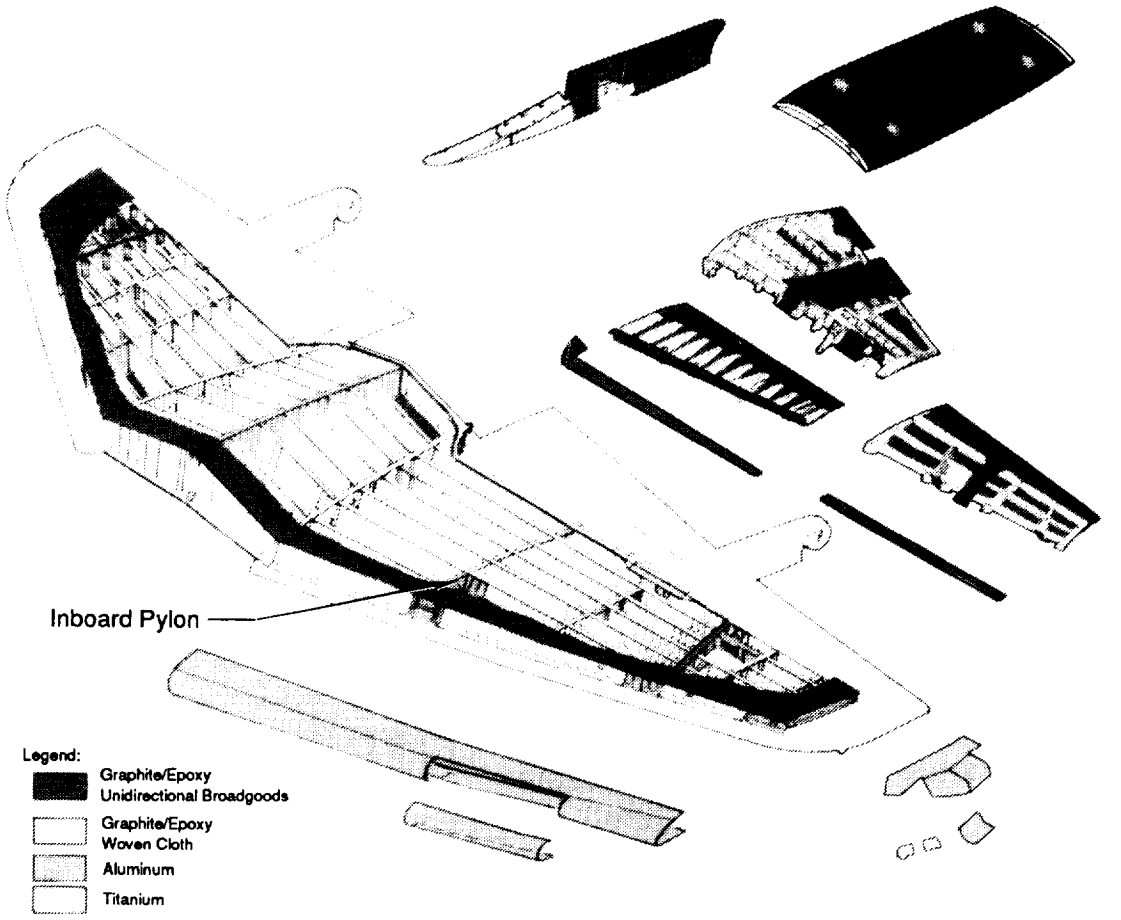

GP11-0332-1/dcb

Figure 1. AV-8B Composite Wing

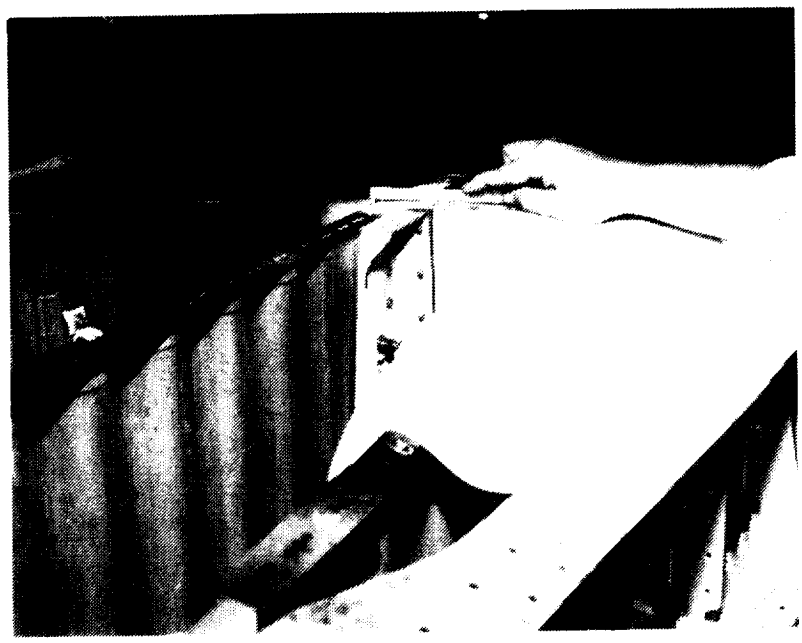

GP11-0332-2/dcb

Figure 2. Substructure at Inboard Pylon

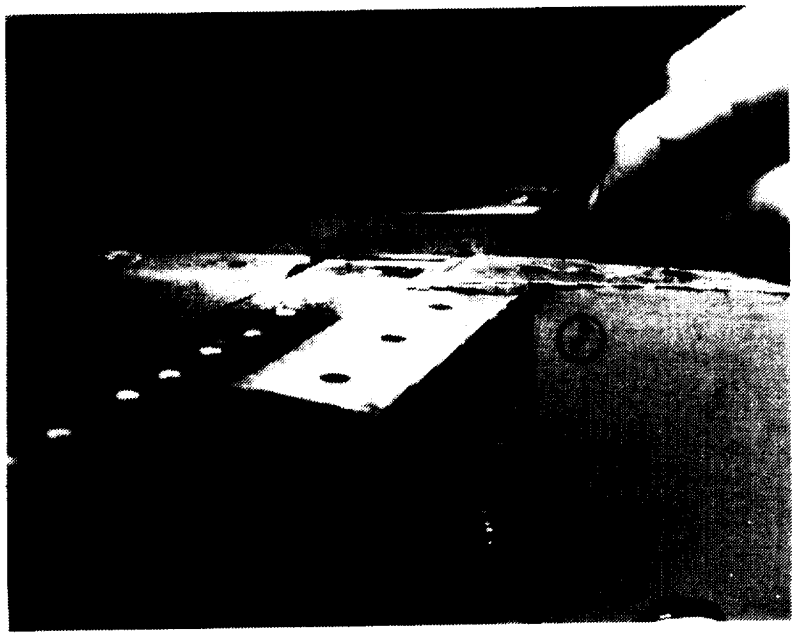

GP11-0332-3/dcb

Figure 3. Close Up of Substructure at Inboard Pylon

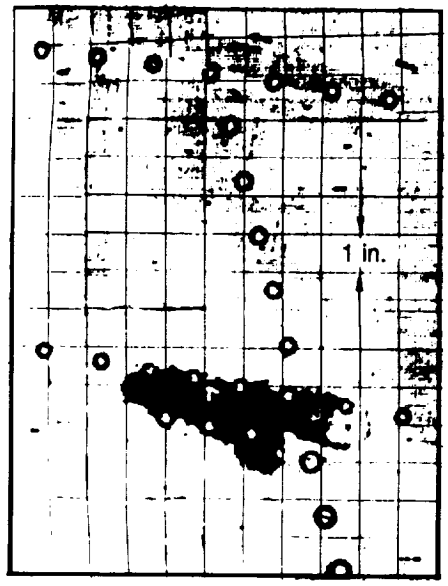

GP11-0332-4/dcb

Figure 4. Ultrasonic Portrait of Skin Delamination

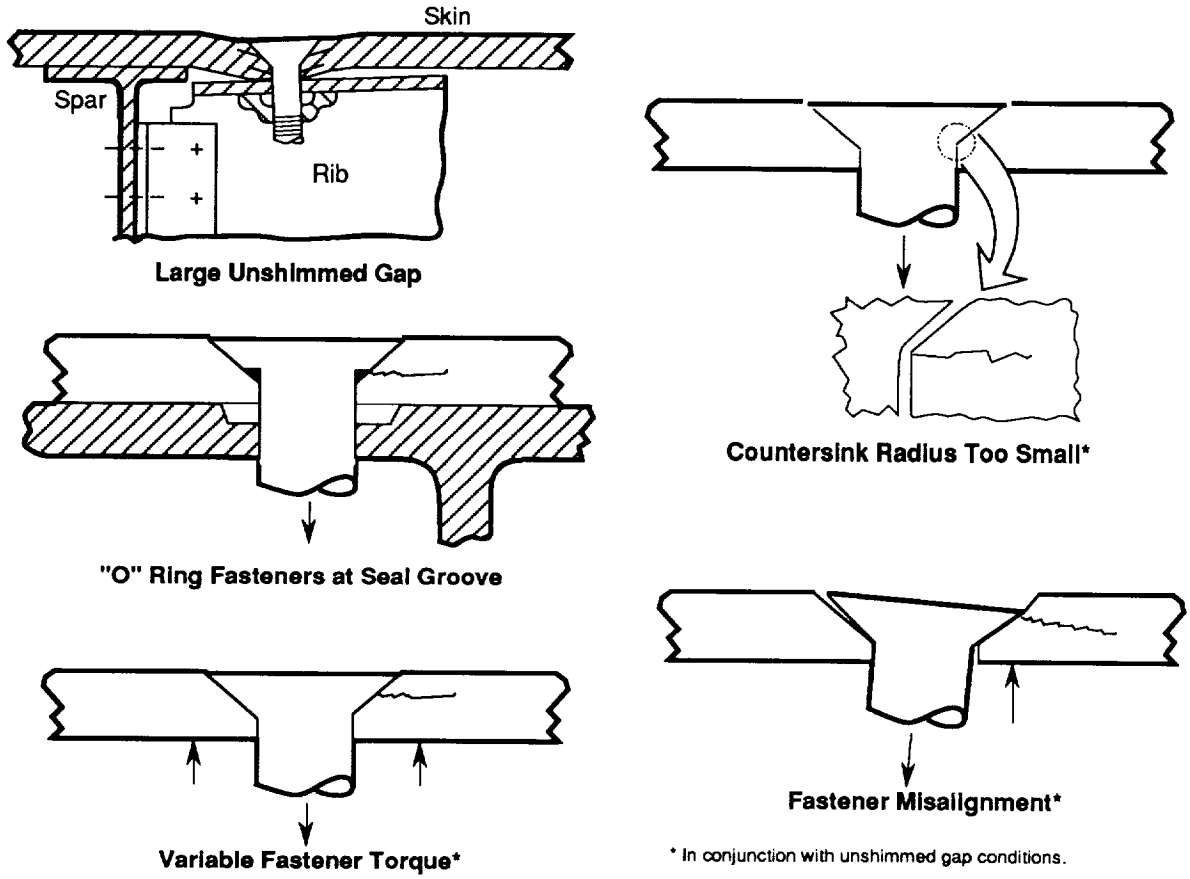

GP11-0332-8-D/dcb

Figure 5. Combination of Factors Caused Delaminations at Fasteners

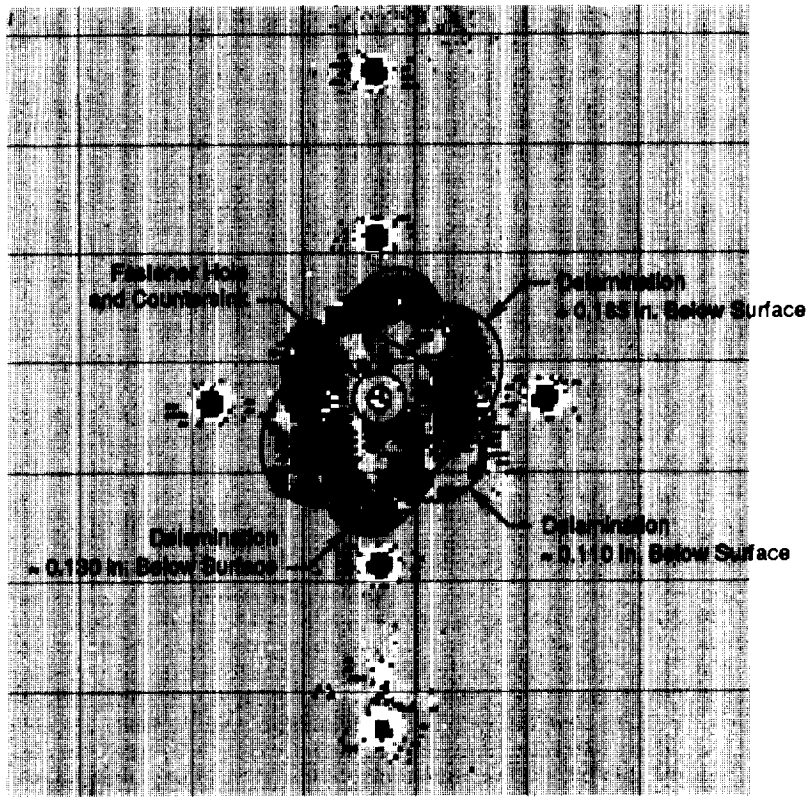

GP11-0332-5/dcb

Figure 6. A-Scan of Typical Fastener Induced Delamination

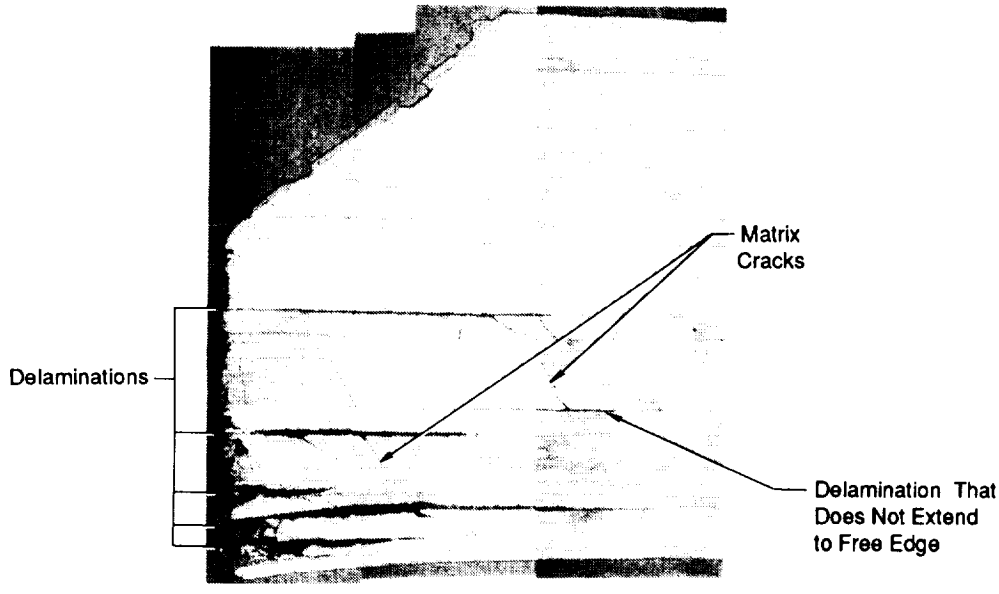

GP11-0332-6-D/dcb

Figure 7. Photomicrograph of Typical Fastener Induced Delamination

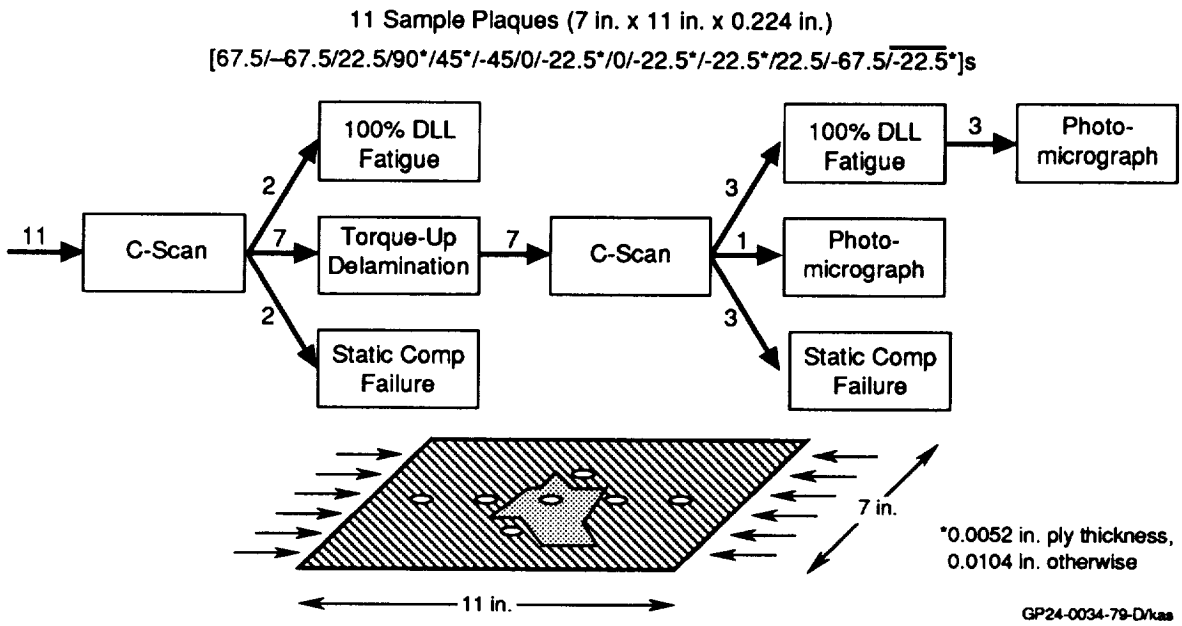

Figure 8. AS4/PEEK and AS4/8551 Test Plan

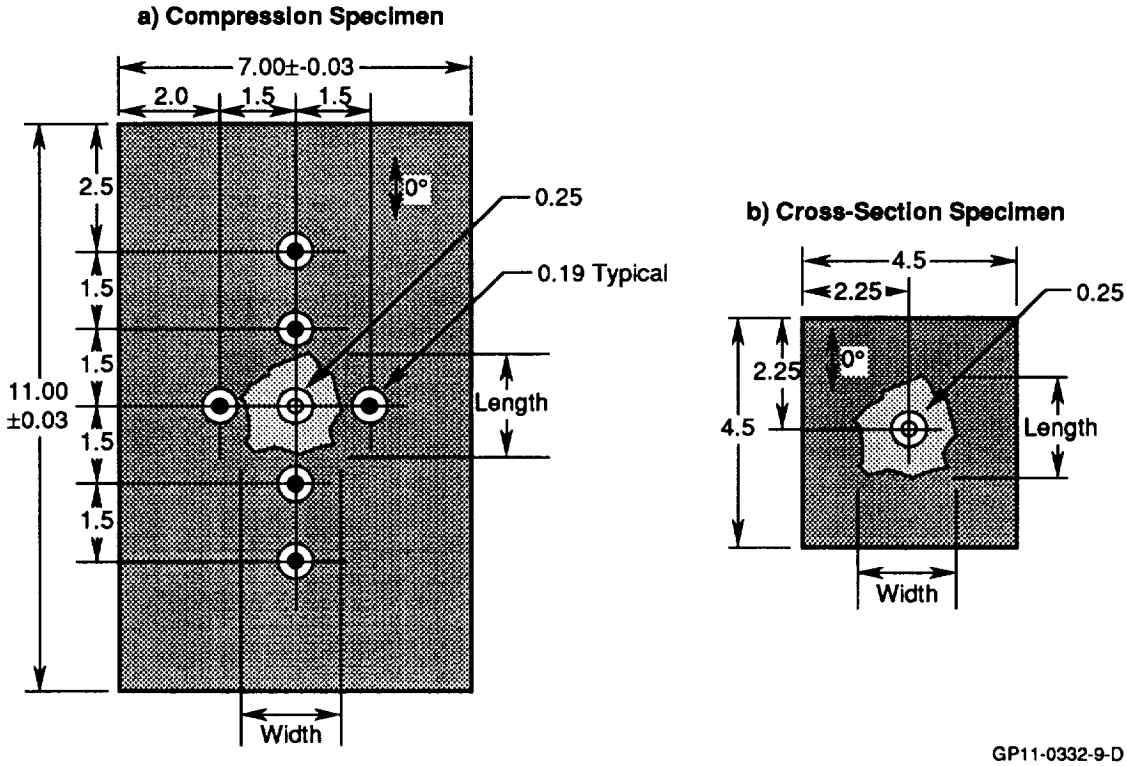

Figure 9. Test Specimens

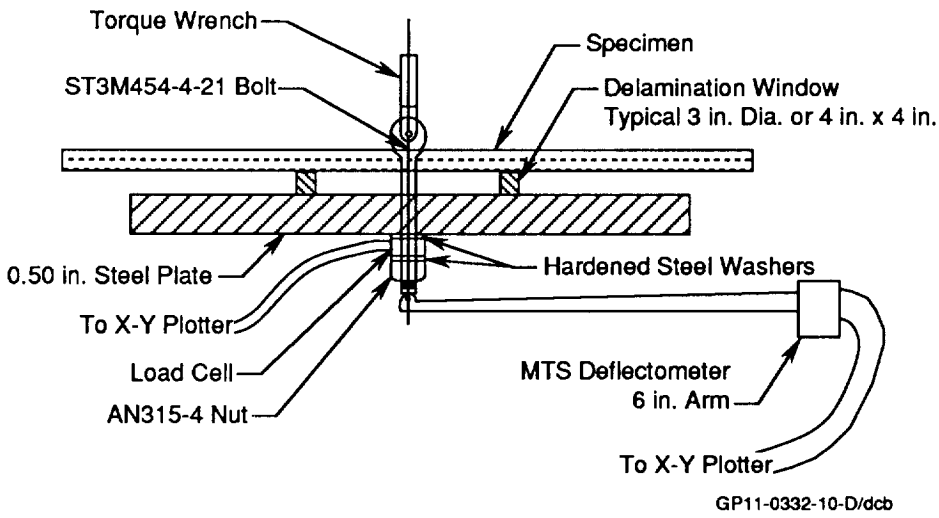

Figure 10. Delamination Setup

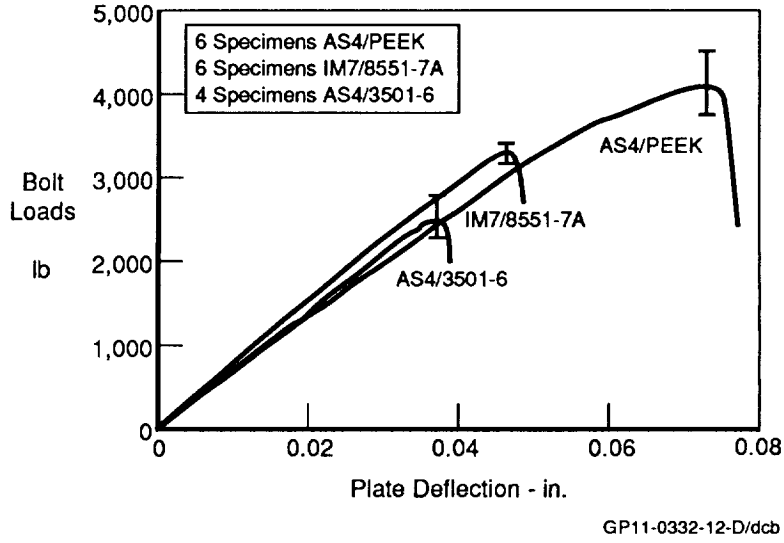

Figure 11. Typical Transverse Load vs Plate Deflection Plots

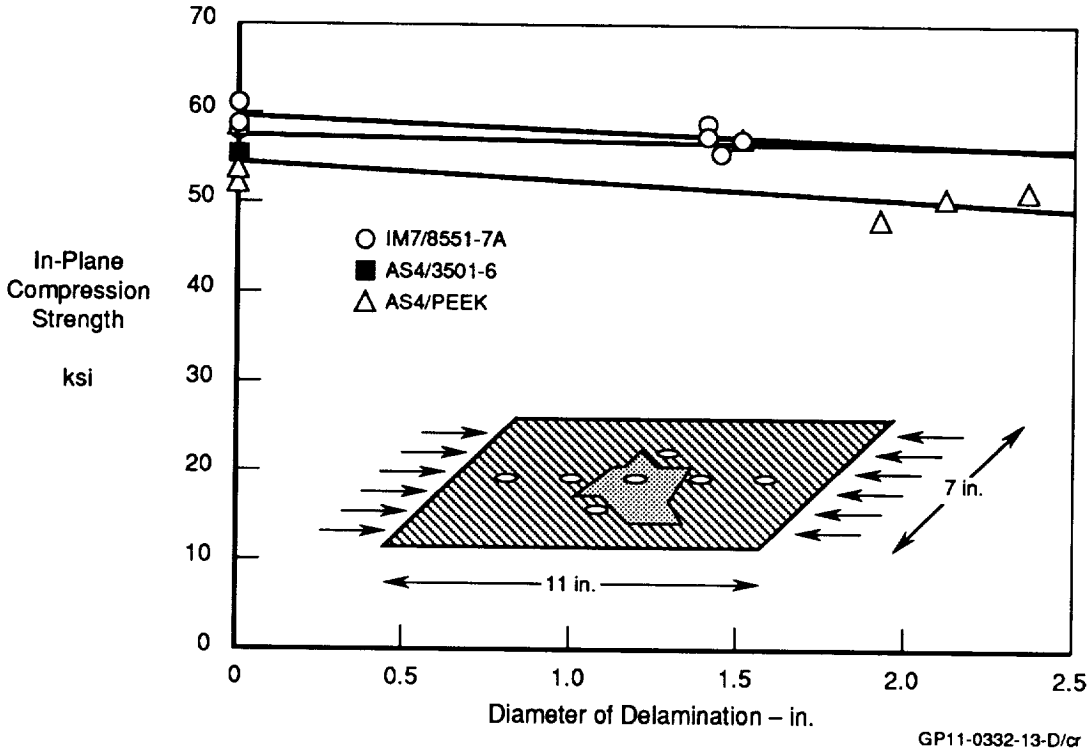

Figure 12. Comparison of the Post Delamination Compression Strength

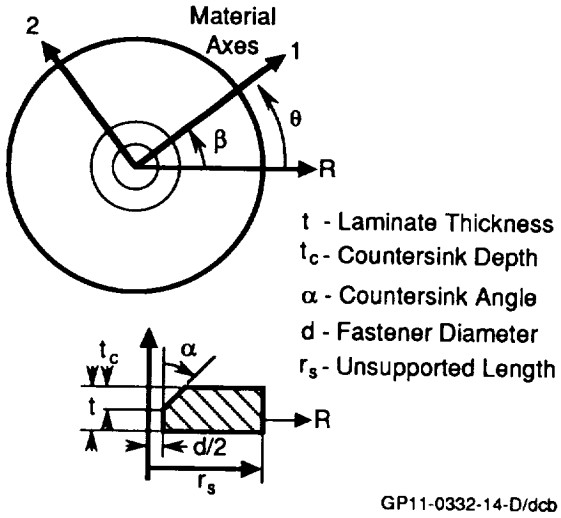

Figure 13. Fastener Hole Analysis Model Nomenclature

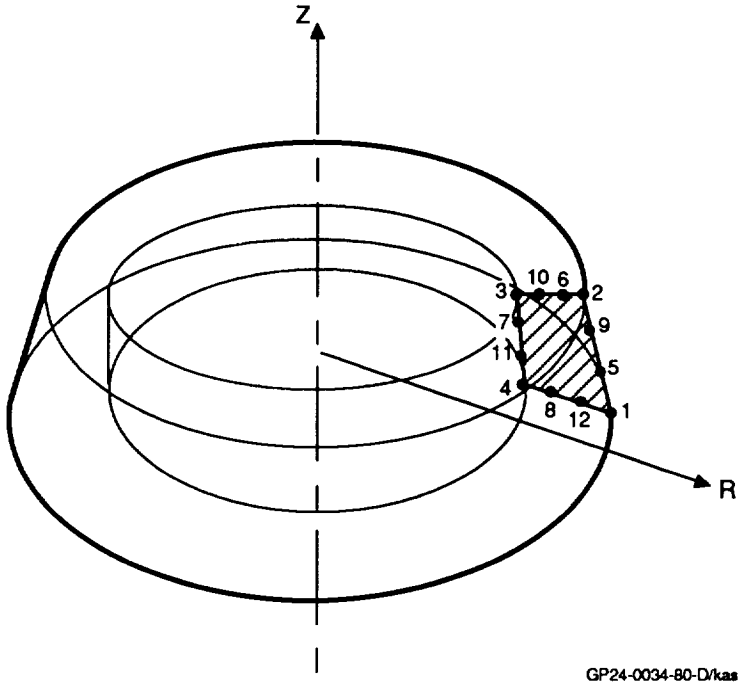

Figure 14. Node Locations for the Anisotropic Harmonic Axisymmetric Element

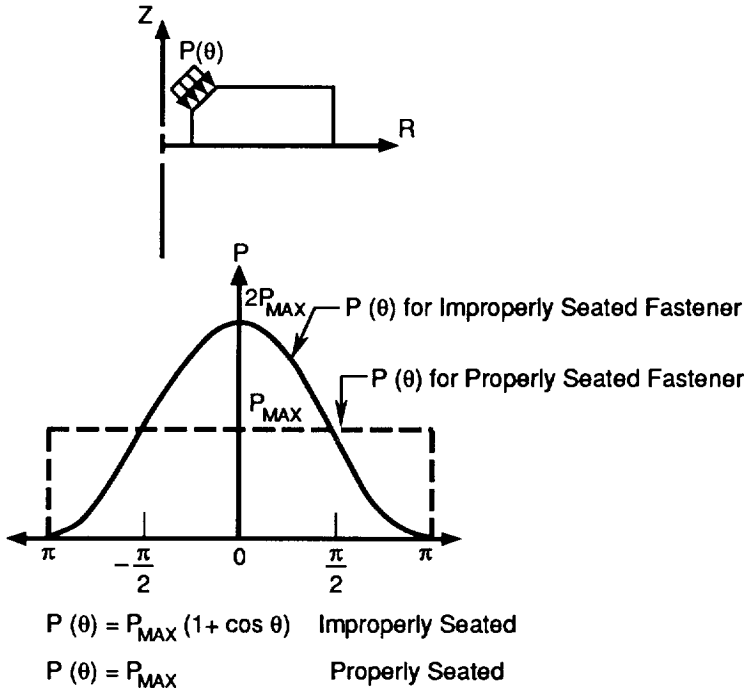

Figure 15. Load Cases for the Fastener Hole Analysis Model

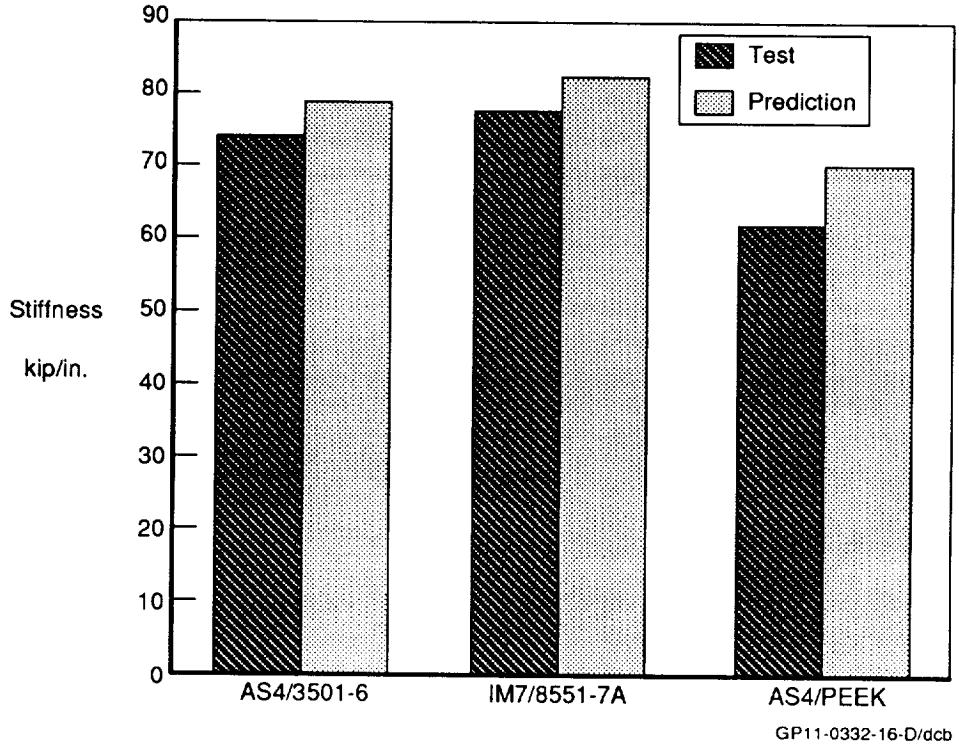

Figure 16. Effective Stiffness Comparisons

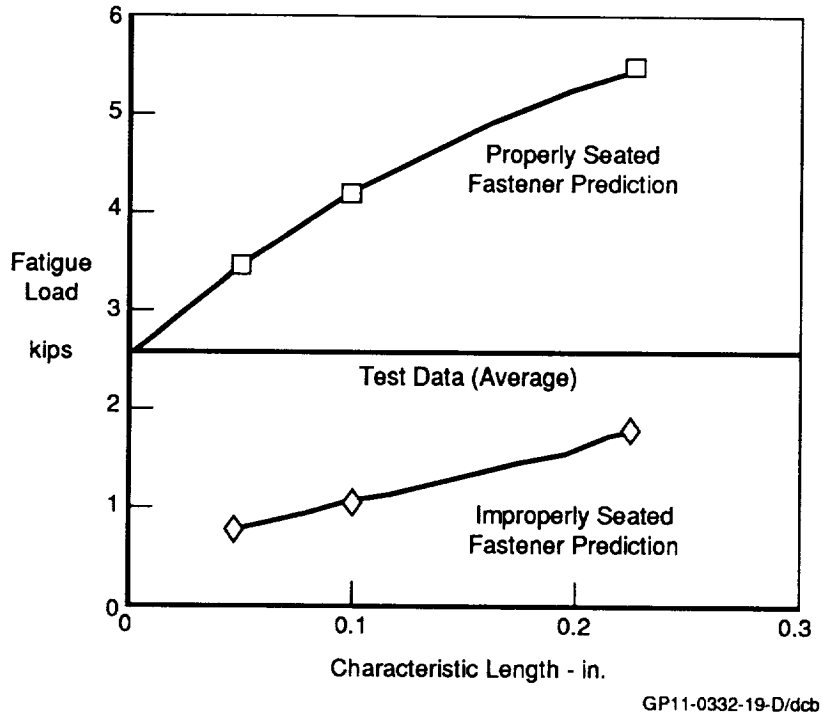

Figure 17 Initial Delamination Load Comparison for an AS4/3501-6 Laminate

TABLE 1. MODES REQUIRED FOR VARIOUS ANALYSIS CASES

Case	D*	Fastener Seating	β	Required Modes
I	Isotropic	Proper	–	0
II	Isotropic	Improper	–	0 and 1st Sym.
III	Orthotropic	Proper	–	0 and Even Sym.
IV	Orthotropic	Improper	0	0 and All Sym.
V	Orthotropic	Improper	≠0	All

GP11-0332-17-D/dcb

TABLE 2. PARAMETERS FOR THE ANALYSIS VERIFICATION MODEL

Parameter	Value
d (in.)	0.25
t_c (in)	0.1080
α (°)	50
t (in.)	0.2236
r_s (in.)	1.5

Stacking Sequence -
[±67.5/22.5/90*/45*/–45/0/(–22.5*)2/22.5/–67.5/22.5*]s
Ply Thickness = 0.0104 in.
* Ply Thickness = 0.0052 in.

GP11-0332-18-D/dcb

THIS PAGE INTENTIONALLY BLANK